ACS APPLIED ENERGY MATERIALS

www.acsaem.org Article

Interface Engineering of Mesoscopic Perovskite Solar Cells by Atomic Layer Deposition of Ta_2O_5

Rohit D. Chavan, Mohammad Mahdi Tavakoli, Suverna Trivedi, Daniel Prochowicz, Abul Kalam, Pankaj Yadav, Pravin H. Bhoite, and Chang Kook Hong*

Cite This: *ACS Appl. Energy Mater.* 2021, 4, 10433−10441 Read Online

ACCESS | Metrics & More | Article Recommendations | Supporting Information

ABSTRACT: Surface passivation of perovskite solar cells (PSCs) has been considered as an effective way to improve the efficiency and stability of devices. Here, we study the influence of an ultrathin layer of tantalum pentoxide (Ta_2O_5) as a passivation layer in the mesoscopic heterojunction PSCs. This material was conformally coated on top of mesoporous TiO_2 (mp-TiO_2) with various thicknesses by the atomic layer deposition technique. We observe that Ta_2O_5 reduces the recombination at the perovskite/mp-TiO_2 contact surface and improves the charge transport, as proved by photoluminescence spectroscopies. With an optimized thickness of Ta_2O_5 (∼1.9 nm), a high-power conversion efficiency of 21.25% was obtained for the Ta_2O_5-modified device, mostly because of the enhancement of the open-circuit voltage (V_{oc}). In addition, our modified cell exhibits low hysteresis, improved shelf life, and thermal and UV light stabilities compared to the unmodified device. Our study demonstrates the importance of surface passivation in mesoscopic PSCs.

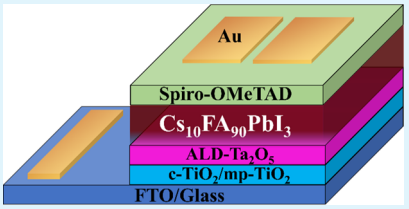

KEYWORDS: *atomic layer deposition, mesoporous-TiO_2, hysteresis, recombination, stability, efficiency*

INTRODUCTION

Hybrid organic−inorganic perovskites have made a revolution in the field of optoelectronic devices over the past decade.[1,2] Particularly, their application in the new generation thin-film solar cells has been significantly highlighted, thanks to their excellent optoelectronic properties, low-cost processing, and ease of manufacture.[3−5] The efficiency of so-called perovskite solar cells (PSCs) has grown rapidly these days and surpassed the power conversion efficiencies (PCEs) of well-known thin film photovoltaic (PV) devices, approaching 25.2%.[6−9] Perovskite active layer can be deposited by various approaches such as spin coating, coevaporation, chemical vapor deposition (CVD), vacuum sequential deposition, and spray-deposition.[10−13] Among them, spin coating is the most popular deposition way due to the ease of processing and low cost. Besides the active layer, electron transporting layers (ETLs) and hole transporting layers have vital roles in both the PCE and stability of the PSCs, and material selection has to be taken into consideration precisely in terms of either charge transfer properties or band alignment.[14−16] Mesoscopic PSCs, one of the most popular device architecture in the perovskite field, is commonly fabricated on the mesoporous TiO_2 (mp-TiO_2) scaffold showing great performance.[17−20] Since mp-TiO_2 has a large surface area with possibly many surface defects, the chance of contact surface recombination would be high, and therefore, surface treatment of mp-TiO_2 is crucial to improve the open-circuit voltage (V_{OC}) as well as device stability.[21] For this purpose, mp-TiO_2 was doped with different metal cations in order to reduce the resistance and improve the conductivity.[22,23] Moreover, various passivation layers have been developed to properly reduce the surface defects of mp-TiO_2. For instance, the ultrathin layers of SnO_2, ZnO, Al_2O_3, ZrO_2, CdS, Sb_2S_3, ZnS, TiN, MgO, and La_2O_3 showed great potential for improvement of the PV performance of the mesoscopic PSCs, mainly due to better band alignment and charge extraction properties.[7,24−27]

Tantalum pentoxide (Ta_2O_5) is a promising n-type material owing to its low leakage current, good electron conductivity, and high thermal as well as chemical stability properties.[28,29] Ta_2O_5 is extensively used in the production of capacitors owing to its high dielectric constant.[30] It is also transparent to incident solar radiation owing to its large band gap (E_g = 3.8 eV). Recently, Ta_2O_5 layer (hole-blocking) has demonstrated effectiveness in minimizing charge recombination and enhancing the PCE in indium phosphide solar cells.[31] Notably, to the best of our knowledge, there is not any report regarding the application of Ta_2O_5 in PSCs. Generally, the Ta_2O_5 film is deposited by CVD, electron-beam evaporation, RF sputtering, or by thermal oxidation technique.[32] However, atomic layer deposition (ALD) would be an interesting approach to develop thin film formation due to the great advantages of this technique including deposition of a high-quality thin film with

Received: February 4, 2021
Accepted: September 22, 2021
Published: October 6, 2021

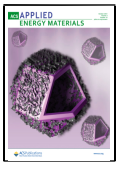

https://doi.org/10.1021/acsaem.1c00367
ACS Appl. Energy Mater. 2021, 4, 10433−10441

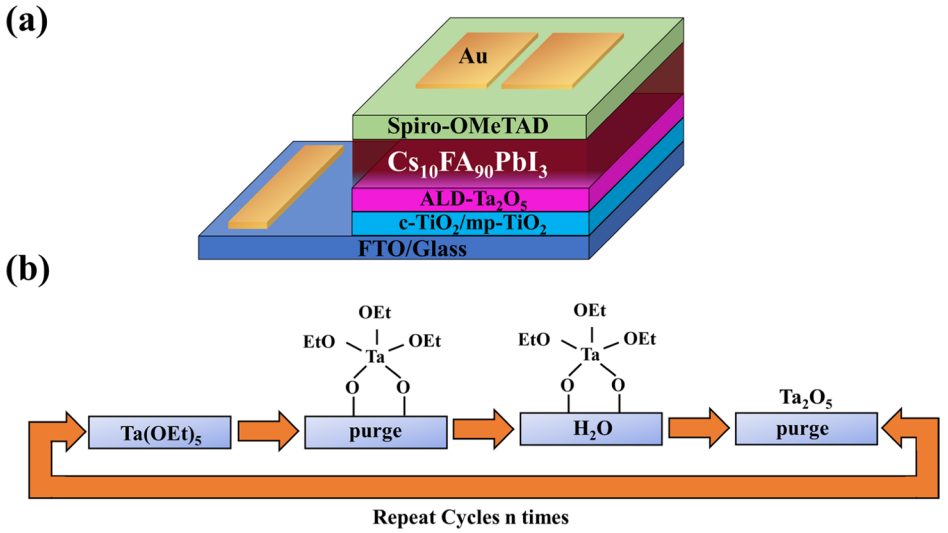

Figure 1. (a) Schematic illustration of the investigated mesoscopic PSCs. (b) Schematic of the ALD deposition of Ta_2O_5 on the surface of the mp-TiO_2 scaffold.

great accuracy in uniformity and thickness and superior electrical and optical performances.[33−36]

Herein, we introduce an ultrathin layer of Ta_2O_5 on top of mp-TiO_2 using the ALD process and investigate its role in the changes in efficiency and stability of the PSCs. This modification results in a lower carrier recombination rate and enhanced charge-transfer properties, as proved by time-resolved photoluminescence spectroscopy (TRPL) and ultraviolet photoelectron spectroscopy (UPS). With an optimized thickness of Ta_2O_5 (1.9 nm), a PSC with a maximum PCE of 21.25% [circuit current density (J_{sc}) = 23.52 mA cm^{-2} and a fill factor (FF) = 78.28%] and negligible hysteresis was achieved. The high V_{OC} of 1.16 V in the Ta_2O_5-modified PSC as compared to the reference cell (1.11 V) indicates the great potential of Ta_2O_5 for reducing the contact surface recombination, as also supported by electrochemical impedance spectroscopy (EIS) and Mott−Schottky (MS) measurements. Finally, the Ta_2O_5-modified PSC shows excellent shelf-life stability by maintaining 85% of the original PCE after 700 h storage in ambient air, which is superior to that of the reference cell (60%). In addition, the modified cell shows enhanced thermal stability at 85 °C and under constant UV light irradiation.

EXPERIMENTAL SECTION

Materials. All solvents and perovskite precursors with super dehydrated grade were purchased from a commercial vendor (Sigma-Aldrich).

Solar Cell Preparation. The etched FTO glass substrates were ultrasonically cleaned with soap, deionized water, ethanol, and isopropanol for 20 min separately. Then, the substrates were treated by UV ozone for 15 min. Following this step, a compact 20 nm layer of TiO_2 (c-TiO_2) was deposited by the spin-coating method.[22] Afterward, a ∼ 180 nm thick TiO_2 mesoporous layer prepared by ethanol-diluted 3 NR paste (1:6 by weight) was spin coated at 4000 rpm for 30 s and heated at 500 °C for 30 min. The perovskite solution in 1 mL of dimethylformamide/dimethyl sulfoxide solvent mixture in a volume ratio of 4:1 was prepared from FAI (0.172 mg), PbI_2 (0.461 mg), and CsCl (0.016 mg). The perovskite solution was spin-coated onto the substrate at 1000 rpm for 10 s and continuously at 6000 rpm for 30 s[37] During the second step, 150 mL of chlorobenzene was poured on the films for 10 s, and the film was sintered at 150 °C for 30 min. Next, the hole-transporting material solution was prepared by dissolving spiro-OMeTAD in chlorobenzene at 70 mM, where TBP, Li-TFSI in acetonitrile, and FK209 in acetonitrile (molar ratio of spiro/FK209/Li-TFSI/TBP of 1:0.03:0.5:3.3) are added as additives.[38] The gold electrodes (80 nm) were deposited by a thermal evaporation system using high vacuum condition. The active area was defined using a 0.09 cm^2 nonreflective mask.

An ultrathin layer of Ta_2O_5 was formed on mp-TiO_2 using the ALD system (NCD Lucida-D100, Korea). Tantalum pentaethoxide [Ta-$(OEt)_5$] and water (H_2O) were used as precursors for Ta_2O_5 film formation at a temperature around 300 °C. The pulse time for $Ta(OEt)_5$ and H_2O was set as 1.2 s, and the purging time was 15 s. It has been estimated that the deposition rate of Ta_2O_5 is 0.13 nm/cycle, which is confirmed by ellipsometry.

Device Measurement and Characterization. The current−voltage (J−V) scans of the cells were recorded under simulated one-sun AM 1.5 G illumination (100 mW cm^{-2}). The external quantum efficiencies (EQEs) were probed by a DK240 monochromator. The crystal structure of the materials was characterized using powder X-ray diffraction (XRD) with a Cu k line of 1.5410 °(Rigaku, Japan). The morphology and energy dispersive X-ray analysis were probed by field emission scanning electron microscopy (FE-SEM, S-4700 Hitachi). The roughness profile of the perovskite film was obtained from a XE-100 advanced scanning probe microscope. UV−vis transmission and absorption spectra of the resulting films were measured by a Cary 300 model system. The oxidation state of the ETL was studied by MultiLab2000 spectrometer. A focused ion beam was applied for the cross-sectional mp-TiO_2/Ta_2O_5 film analysis using a transmission electron microscope (FEI, Helios G3 CX). A four-point probe instrument (Hall measurement) was used to measure the conductivity of the ETLs. UPS spectra are gathered using HeI irradiation with $h\nu$ = 21.22 eV produced by a UV source (Axis-Supra). The PL properties were analyzed with a fluorescence MicroTime-200 spectrometer (Picoquant, Germany). EIS analysis was carried out at 0 bias and under dark condition.

RESULTS AND DISCUSSION

The conventional mesoporous configuration of the PSC with $Cs_{0.1}FA_{0.9}PbI_3$ as an absorber active layer[37] was used to study the effect of ETL functionalization on the device performance and stability (Figure 1a). We have previously demonstrated that the introduction of an ultrathin passivation layer on the surface of mp-TiO_2 improves its electron-transfer properties.[27,39,40] Wide band gap Ta_2O_5 is regarded as the material having high electrical conductivity and good stability.[28,29]

https://doi.org/10.1021/acsaem.1c00367
ACS Appl. Energy Mater. 2021, 4, 10433−10441

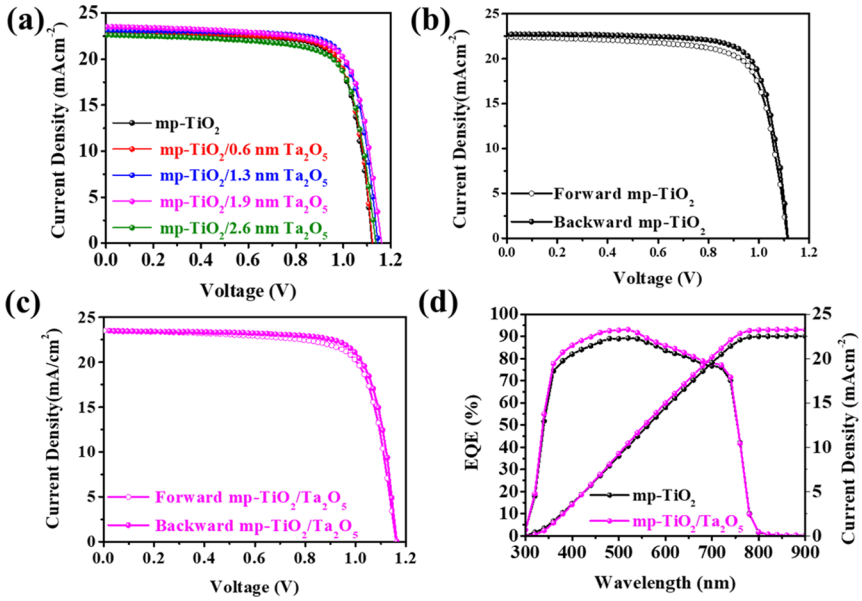

Figure 2. (a) $J-V$ curves of the devices based on mp-TiO_2 and mp-TiO_2/Ta_2O_5 ETL with different thicknesses of Ta_2O_5 (scan rate 50 mV s^{-1}). The hysteresis of $J-V$ curves of the device based on (b) mp-TiO_2 and (c) mp-TiO_2/Ta_2O_5 ETLs. (d) EQE spectra of the devices based on mp-TiO_2 and (c) mp-TiO_2/Ta_2O_5 ETLs.

Table 1. PV Output of the Devices Based on mp-TiO_2 and mp-TiO_2/Ta_2O_5 ETLs under AM 1.5 G Illumination with Varying Thicknesses of the Ta_2O_5 Layer (Scan Rate 50 mV s^{-1})

ETLs		V_{oc} [V]	J_{sc} [mA/cm^2]	FF	PCE [%]
mp-TiO_2	champion	1.115	22.70	75.72	19.02
	average	1.105 ± 0.010	22.3 ± 0.4	73 ± 2.5	18.60 ± 0.4
mp-TiO_2/0.6 nm Ta2O5	champion	1.123	22.84	76.83	19.58
	average	1.110 ± 0.010	22.4 ± 0.4	74 ± 2.5	19.2 ± 0.4
mp-TiO_2/1.3 nm Ta_2O_5	champion	1.131	23.10	77.21	20.10
	average	1.120 ± 0.010	22.5 ± 0.30	75 ± 2.0	19.8 ± 0.3
mp-TiO_2/1.9 nm Ta_2O_5	champion	1.160	23.52	78.28	21.25
	average	1.150 ± 0.007	23.30 ± 0.20	76 ± 2.0	20.90 ± 0.3
mp-TiO_2/2.6 nm Ta_2O_5	champion	1.035	22.63	74.35	19.37
	average	1.020 ± 0.015	22.2 ± 0.4	71 ± 3.0	19.0 ± 0.4

Having in mind that higher conductivity signifies better charge transport, we first attempted to investigate the changes in electrical conductivity of mp-TiO_2 after functionalization with Ta_2O_5. The surface of mp-TiO_2 was coated by the Ta_2O_5 layer with different thicknesses using the ALD technique. The schematic of ALD process for the formation of Ta_2O_5 with the help of $Ta(OEt)_5$ and H_2O is shown in Figure 1b.[41] By altering the number of deposition cycles, the mp-TiO_2/Ta_2O_5 films with 0.65, 1.3, 1.9, and 2.6 nm thicknesses were formed. The effect of Ta_2O_5 film thickness on the electrical properties of ETL is examined by Hall measurement. We found that the film with the 1.9 nm thick Ta_2O_5 layer exhibits better conductivity as compared to other films (Table S1). Moreover, we compared the electrical properties of the mp-TiO_2/Ta_2O_5 film (1.9 nm) with the mp-TiO_2 films functionalized with ALD-deposited TiN[32] and Nb_2O_5,[47] which we previously optimized and reported (Table S2). The mp-TiO_2/Ta_2O_5 film has a higher conductivity than other films of similar thicknesses, which indicates that this functionalization should enhance the charge transport across the ETL/perovskite contact surface and consequently further boost the performance of mesoscopic PSCs.

To confirm the presence of Ta_2O_5 on top of the bare mp-TiO_2, FE-SEM and X-ray photoelectron spectroscopy (XPS) analyses were carried out. Figure S2 shows the plain-view FE-SEM images of the bare mp-TiO_2 and mp-TiO_2 with Ta_2O_5, indicating the presence of highly dense TiO_2 nanoparticles. The regular distributions of Ti, O, and Ta elements on top of mp-TiO_2 is revealed by the EDS analysis (Figure S3). In addition, transmission electron microscopy (TEM) analysis of mp-TiO_2/Ta_2O_5 ETL reveals the presence of the 2.0 nm thick Ta_2O_5 compact layer on top of the mp-TiO_2 ETL (Figure S4). The surface of the films was further probed by XPS measurements (Figure S5). The XPS spectrum survey of mp-TiO_2/Ta_2O_5 confirms the presence of Ti, O, and Ta elements on top of the mp-TiO_2 scaffold (Tables S3 and S4). The Ta $4f_{7/2}$ core level spectrum of the mp-TiO_2/Ta_2O_5 film shows two peaks located at 25.06 and 27.01 eV corresponding to Ta_2O_5.[42,43] In turn, the Ti 2p core level spectrum of the mp-TiO_2 film demonstrates two peaks with binding energies of 458.40 and 463.52 eV, which relate to Ti(IV) of anatase TiO_2.[22] These peaks slightly shift toward a higher binding energy in the mp-TiO_2/Ta_2O_5 sample. Similarly, the peak of the O 1s binding energy shifts from 529.72 to 529.91 eV after Ta_2O_5 functionalization. The observed shift toward high

https://doi.org/10.1021/acsaem.1c00367
ACS Appl. Energy Mater. 2021, 4, 10433−10441

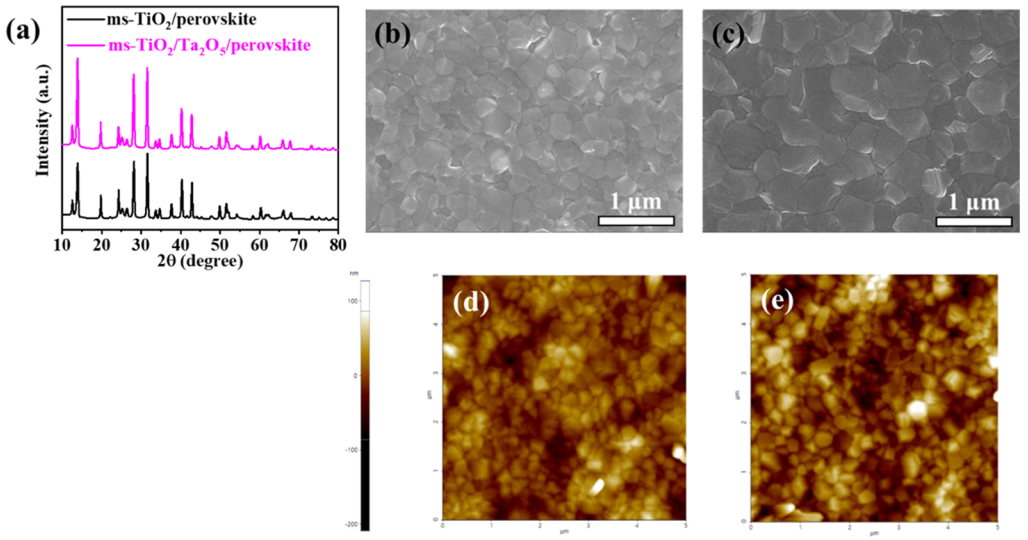

Figure 3. (a) XRD peaks of the perovskite films deposited on mp-TiO_2 and mp-TiO_2/Ta_2O_5 ETLs. Plain view FE-SEM of the (b) mp-TiO_2/perovskite and (c) mp-TiO_2/Ta_2O_5/perovskite films. AFM images of the (d) mp-TiO_2/perovskite and (e) mp-TiO_2/Ta_2O_5/perovskite films.

binding energy may suggest that some Ti−O−Ta bonds are formed.[44]

To study the role of Ta_2O_5 on the PV properties, devices with mp-TiO_2 and mp-TiO_2/Ta_2O_5 ETLs were fabricated. Figure S6 displays the cross-sectional SEM images of mp-TiO_2- and mp-TiO_2/Ta_2O_5-based PSCs. The thicknesses of the perovskite and spiro-OMeTAD layers in both devices are found to be 400 and 200 nm, respectively. Figure 2a shows the current−voltage (J−V) curves of the PSCs with various thicknesses of Ta_2O_5 measured under standard AM 1.5 G condition and reverse scan (scan rate 50 mV s^{-1}). Table 1 summarizes the PV parameters of the champion devices. The reference cell shows the highest PCE of 19.02% with a V_{oc} of 1.11 V, J_{sc} of 22.70 mA cm^{-2}, and FF of 75.72%. We found that by deposition of Ta_2O_5 on mp-TiO_2 with an optimized thickness of ∼1.9 nm, the PCE is increased up to a maximum value of 21.25% with a V_{oc} of 1.16 V, J_{sc} of 23.52 mA, cm^{-2} and FF of 78.28%. However, with the further increase of the film thickness, the performance of the device declines to 19.37%. For checking the reproducibility, 20 independent devices were fabricated under the same conditions. Figure S7 depicts the statistical histogram of PV parameters for the reference and modified devices following the same trend of the best performing devices. To evaluate the PV results of our work with the state-of-art devices based on the modified mp-TiO_2 ETL, we compared the PV parameters of our devices with the best reports in the literature, as can be found in Table S5. The J−V curves of the pristine and Ta_2O_5-modified PSCs in both forward and backward biases are demonstrated in Figure 2b,c, respectively. The hysteresis index (HI) of the corresponding PSCs was determined by the given equation[45]

$$\mathrm{HI} = \frac{\int_0^{V_{oc}} J_R(V)\,\mathrm{d}V - \int_0^{V_{oc}} J_F(V)\,\mathrm{d}V}{\int_0^{V_{oc}} J_R(V)\,\mathrm{d}V}$$

It is found that the device with the mp-TiO_2/Ta_2O_5 ETL exhibits a negligible HI of 1.36%, which is smaller than that of the device based on mp-TiO_2 ETL (2.64%) (Table S6). In general, hysteresis typically occurs in PSCs due to charge or ion accumulation and the imbalance of charge carrier at the contact surface of the perovskite/ETL.[46−48] We found that the presence of Ta_2O_5 between the perovskite layer and the mp-TiO_2 ETL reduces the HI, which we attribute to effective electron extraction at the modified ETL/perovskite contact surface (vide infra). Figure 2d depicts the EQE spectra of the corresponding devices indicating EQE values of above 90% in the entire spectrum. The integrated J_{sc} from EQE results were calculated to be 22.27 and 23.53 mA cm^{-2} for the devices based on mp-TiO_2 and mp-TiO_2/Ta_2O_5 ETL, respectively, which are in good agreement with the J−V results. In addition, the stabilized efficiency and J_{sc} of both devices were investigated near the maximum power point under continuous illumination for 100 s (Figure S8a,b). The device based on mp-TiO_2 and mp-TiO_2/Ta_2O_5 ETL shows stabilized PCEs of 18.7 and 20.9% and J_{sc} values of 22.4 and 23.2 mA cm^{-2}, respectively.

To further investigate the role of Ta_2O_5 layer on the performance of PSCs, we first compare the wettability of our perovskite solution on the investigated scaffolds by contact angle measurements (Figure S9). It can be seen that the mp-TiO_2/Ta_2O_5 film had a lower contact angle of a droplet of perovskite solution, which is beneficial for the preparation of the perovskite film with better quality and uniformity. Besides, the mp-TiO_2/Ta_2O_5 film exhibits a better surface morphology with the root-mean-square (RMS) of 16.35 nm than that of the mp-TiO_2 film with the RMS of 22.80 nm (Figure S10). The smoother surface can also facilitate the crystallization of the perovskite film and improve the ETL/perovskite contact surface. In the next step, we analyze the crystallinity and morphology of the perovskite layer deposited on mp-TiO_2 and mp-TiO_2/Ta_2O_5 ETLs. The XRD patterns of the mp-TiO_2/perovskite and mp-TiO_2/Ta_2O_5/perovskite films are shown in Figure 3a. As seen, both samples display a similar crystal structure, and the higher diffraction peaks for the mp-TiO_2/Ta_2O_5/perovskite sample indicate its improved crystallinity. The peak located at 12.7° is assigned to the PbI_2 phase, which is formed as a consequence of high-temperature annealing.[49,50] The improvement in crystallinity of the perovskite layer was also verified by FE-SEM images as shown in Figure 3b,c. As seen, the perovskite layer deposited on the mp-TiO_2/Ta_2O_5 ETL displays a denser and more homogenous surface

https://doi.org/10.1021/acsaem.1c00367
ACS Appl. Energy Mater. 2021, 4, 10433−10441

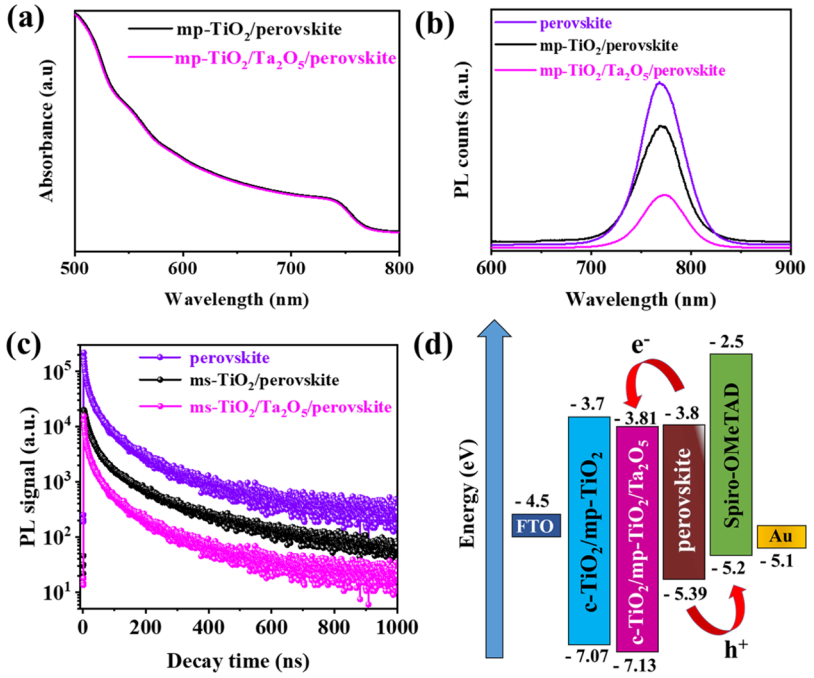

Figure 4. (a) UV−vis absorption, (b) PL, and (c) TRPL spectra. (d) Schematic energy diagram of devices with mp-TiO_2 and mp-TiO_2/Ta_2O_5 ETLs.

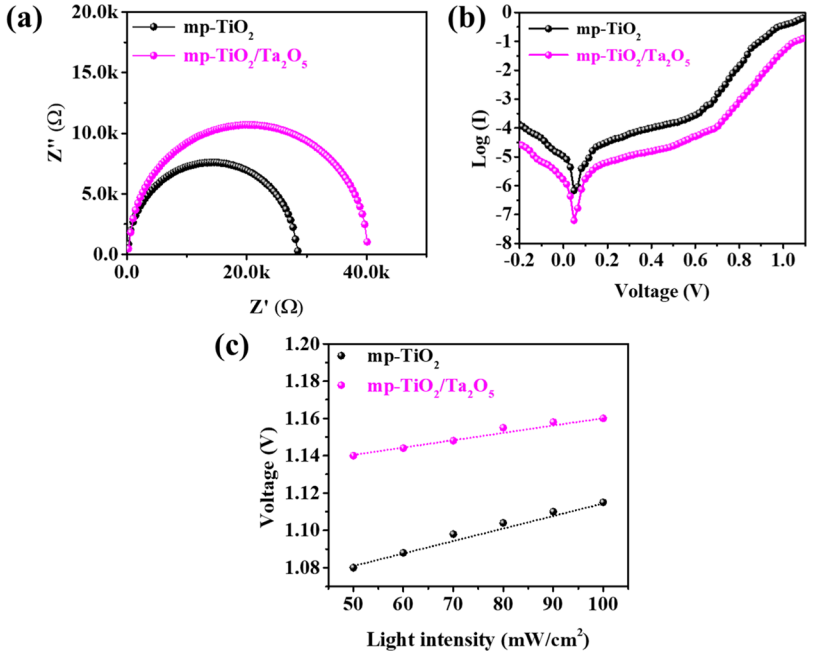

Figure 5. (a) Nyquist plots; (b) dark J−V curves and (c) V_{OC} as a function of light intensity of the devices based on mp-TiO_2 and mp-TiO_2/Ta_2O_5 ETLs.

morphology. Moreover, the average grain size of the perovskite film on mp-TiO_2/Ta_2O_5 (~800 nm) is larger than that of the mp-TiO_2-coated perovskite sample (~500 nm). The observed larger grain size and improved crystallinity can explain the observed lower hysteresis and higher V_{OC} in the device based on mp-TiO_2/Ta_2O_5 ETL.[51,52] The corresponding atomic force microscopy (AFM) images of the perovskite films deposited on mp-TiO_2 and mp-TiO_2/Ta_2O_5 ETLs are shown in Figure 3d,e. It is found that the mp-TiO_2/Ta_2O_5/perovskite sample exhibits a smoother surface with an RMS value of 11.38 nm as compared to the reference film (22.62 nm), which can be beneficial for reducing the contact surface recombination.[53]

To investigate the influence of Ta_2O_5 layer on the optical properties of the perovskite film, the UV−visible, steady-state PL, and TRPL measurements were conducted. Figure 4a shows the UV−visible spectra of the mp-TiO_2/perovskite and mp-TiO_2/Ta_2O_5/perovskite, indicating the absorption with a 1.6 eV optical band gap. However, as depicted in Figure 4b, the perovskite film formed on mp-TiO_2/Ta_2O_5 exhibits stronger PL quenching effect compared to the perovskite film formed on mp-TiO_2 ETL and bare glass. The TRPL spectra of the

https://doi.org/10.1021/acsaem.1c00367
ACS Appl. Energy Mater. 2021, 4, 10433−10441

resulting films follow the same trend as shown in Figure 4c. Indeed, the mp-TiO_2/Ta_2O_5/perovskite film has a shorter carrier lifetime (67 ns) compared to the mp-TiO_2/perovskite film (101 ns). Shorter lifetime here indicates that the electrons move to the ETLs faster before they recombine at the contact surface.[54−56] The fitting parameters of TRPL curves with a biexponential decay function can be found in Table S7. These results suggest a more efficient charge transport from the perovskite absorber to the mp-TiO_2/Ta_2O_5 ETL. UPS was further used to probe the beneficial effect of the Ta_2O_5 layer on the charge transfer in a complete device. Figure S11a displays the UPS spectra of bare mp-TiO_2 and mp-TiO_2 with Ta_2O_5 ETLs. From these results, the valence band of mp-TiO_2 and mp-TiO_2/Ta_2O_5 ETLs were calculated to be −7.07 and −7.13 eV, respectively. The calculated band gap energy of mp-TiO_2 and mp-TiO_2/Ta_2O_5 (optimum thickness) were extracted from the transmission spectra and found to be 3.37 and 3.32 eV, respectively (Figure S1b). Thus, the conduction bands of mp-TiO_2 and mp-TiO_2/Ta_2O_5 ETLs were calculated to be −3.7 and −3.81 eV, respectively. Using these numbers as well as those given in the literature,[52] we plotted the band energy diagram as shown in Figure 4d. A small energy barrier (100 meV) is observed for the electron transfer from the perovskite to the mp-TiO_2 ETL. This barrier can block the electrons and increase the chance of contact surface recombination. However, in the case of the mp-TiO_2/Ta_2O_5 ETL, there is not any barrier for the electron transfer, and the band energy mismatch is only 10 meV. As a result, the presence of Ta_2O_5 at the ETL/perovskite contact surface facilitates the charge transfer and reduces the possibility of contact surface recombination, resulting in a higher V_{OC} in the modified devices.[57−59] The enhancement of V_{oc} in the mp-TiO_2/Ta_2O_5 modified device was also confirmed using MS and EIS measurements. The MS plots measured using a three-electrode system for both the devices are shown in Figure S12. As seen, the presence of Ta_2O_5 negatively shifts the estimated flat band potentials (E_{fb}) from −0.77 to −0.36 V (vs saturated calomel electrode). The negative shift in E_{fb} contributes to higher V_{OC} and enhanced performance of the modified device.[60]

Figure 5a depicts the Nyquist plots of the devices with mp-TiO_2 and mp-TiO_2/Ta_2O_5 ETLs measured under dark condition and a zero bias. The equivalent circuit of the device is shown in Figure S13, where R_S, R_{rec}, and C correspond to the series resistance, recombination resistance, and chemical capacitance, respectively. From the results, the device with the mp-TiO_2/Ta_2O_5 ETL has lower R_S (58 Ω) as compared to the device based on mp-TiO_2 ETL (97 Ω), which might illustrate the maximum value of FF in the modified device. The calculated values of R_{rec} are 28,533 and 40,161 Ω for the devices based on mp-TiO_2 and mp-TiO_2/Ta_2O_5 ETLs, respectively. These results suggest that the device with the mp-TiO_2/Ta_2O_5 ETL has a lower interfacial recombination rate as related to the device with the mp-TiO_2 ETL as the R_{rec} rate is inversely proportional to the recombination. The lower contact surface recombination can support the higher V_{OC} in the PSCs with the mp-TiO_2/Ta_2O_5 ETL. In addition, we recorded the dark J−V curves of both the devices, as illustrated in Figure 5b. As seen, the device with the mp-TiO_2/Ta_2O_5 ETL has a smaller leakage current compared to the reference cell, which can also support the higher V_{OC} in these devices. To evaluate the recombination dynamics in the investigated devices, we analyzed the light intensity dependence of V_{OC} by employing the linear expression of $V_{OC} = n(k_BT/q)\ \ln(I) +$ constant (n = ideality factor, k_B = Boltzmann constant, T = absolute temperature, q = charge, and I = light intensity).[61−63] The lower slope of k_BT/q for the mp-TiO_2/Ta_2O_5-based PSC (n = 1.45) suggests a decrease in the trap-assisted recombination process for the perovskite/ETL contact surface compared to the reference cell (n = 1.81) (Figure 5c).

One of the main challenges for PSCs is the improvement of their stability.[64,65] The presence of trap states at the surface of the mp-TiO_2 scaffold is well known to cause high recombination rates of photogenerated electron−hole pairs, which decreases the PSC efficiency and system stability.[66,67] Passivation of the TiO_2 surface defects (Ti^{3+} sites and oxygen vacancies) is a convenient way to suppress the photogenerated charge carrier recombination and improve the device stability.[39,55,68] Here, we evaluate the role of Ta_2O_5 layer on the stability of device without any encapsulation. The results of shelf-life stability for the reference and modified PSCs are shown in Figure 6a. In this experiment, the devices were stored

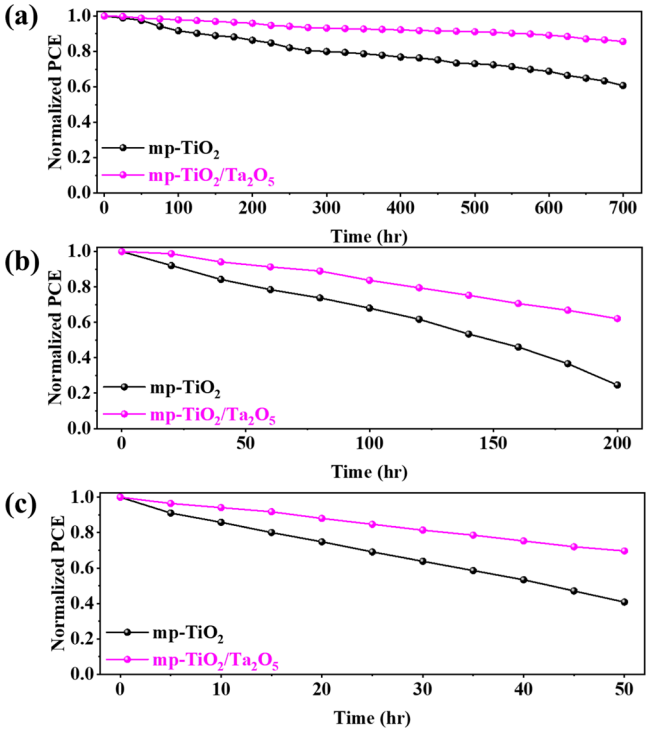

Figure 6. (a) Shelf-life stability test of the unencapsulated devices based on mp-TiO_2 and mp-TiO_2/Ta_2O_5 ETLs at ambient condition (RH ∼ 50%) for 700 h. (b) Thermal stability of the unencapsulated devices based on mp-TiO_2 and mp-TiO_2/Ta_2O_5 ETLs at 85 °C and (c) UV stability of the corresponding PSCs under continuous UV light illumination for 200 h.

at room temperature in ambient air [∼ 50% relative humidity (RH)], and the PV parameters were recorded over 700 h. We found that the device with the mp-TiO_2/Ta_2O_5 ETL retains 85% of its original PCE number; however, the PCE of the device based on mp-TiO_2 ETL maintains 60% of its original PCE. Figure S14 shows the evolution of the average efficiency obtained from four independent devices confirming good reproducibility and stability improvement after mp-TiO_2 surface modification. We also probed the thermal stability of our devices at 85 °C for 200 h (Figure 6b). The modified PSC reaches 62% of its original PCE, while the PCE of the reference cell drops dramatically to 25% in the same condition. As Ta_2O_5

https://doi.org/10.1021/acsaem.1c00367
ACS Appl. Energy Mater. 2021, 4, 10433−10441

has a large band gap, we anticipated that this layer at the ETL/perovskite contact surface can protect the device from the harmful UV light. To confirm the improved stability, we irradiated the devices with mp-TiO_2 and mp-TiO_2/Ta_2O_5 ETLs with continuous UV illumination for 50 h (Figure 6c). Indeed, the device with the mp-TiO_2/Ta_2O_5 ETL was more stable than the reference device, retaining 70% of its initial PCE. These results obviously confirm the beneficial role of the Ta_2O_5 layer on the stability of the mp-TiO_2 PSCs. We attribute the improved operational stability of the modified device to the better quality of the perovskite film and the enhanced contact surface charge-transfer efficiency.

CONCLUSIONS

In summary, we demonstrated the surface modification of the mp-TiO_2 scaffold in mesoscopic PSCs with the ALD-deposited Ta_2O_5 layer. This modification improves the interfacial contact between the ETL and the perovskite absorber layer leading to the perovskite film with higher crystallinity and larger grains. In addition, we showed that the Ta_2O_5 layer suppresses the contact surface recombination and facilitates the charge transfer between the ETL and perovskite absorber due to a better band energy alignment. With an optimum thickness of Ta_2O_5 (~1.9 nm), the high-efficient cell with a maximum PCE of 21.25% and negligible hysteresis was achieved, which is greater than that of the reference device with a PCE of 19.11%. The enhancement of efficiency is primarily due to the improved V_{OC} from 1.11 to 1.16 V. The EIS and MS measurements supported the observed increase in V_{oc} of the modified device. Besides the higher efficiency, the modified device shows excellent shelf-life and thermal and UV stabilities, highlighting the role of the Ta_2O_5 layer for commercialization purposes.

ASSOCIATED CONTENT

Supporting Information

The Supporting Information is available free of charge at https://pubs.acs.org/doi/10.1021/acsaem.1c00367.

Transmission spectra; plain view SEM images; TEM images; XPS spectra; cross-sectional SEM images; PV statistics; steady-state photocurrent and PCE stabilities; contact angle measurement; AFM images; UPS spectra; and MS plots (PDF)

AUTHOR INFORMATION

Corresponding Author

Chang Kook Hong − *Polymer Energy Materials Laboratory, School of Applied Chemical Engineering, Chonnam National University, Gwangju 61186, South Korea;* orcid.org/0000-0001-8663-4490; Email: hongck@chonnam.ac.kr

Authors

Rohit D. Chavan − *Polymer Energy Materials Laboratory, School of Applied Chemical Engineering, Chonnam National University, Gwangju 61186, South Korea*

Mohammad Mahdi Tavakoli − *Department of Electrical Engineering and Computer Science, Massachusetts Institute of Technology, Cambridge, Massachusetts 02139, United States;* orcid.org/0000-0002-8393-6028

Suverna Trivedi − *Department of Chemical Engineering, National Institute of Technology, Rourkela 769008, India*

Daniel Prochowicz − *Institute of Physical Chemistry, Polish Academy of Sciences, Warsaw 01-224, Poland;* orcid.org/0000-0002-5003-5637

Abul Kalam − *Department of Chemistry, Faculty of Science, King Khalid University, Abha 61413, Saudi Arabia*

Pankaj Yadav − *Department of Solar Energy, School of Technology, Pandit Deendayal Petroleum University, Gandhinagar, Gujarat 382 007, India;* orcid.org/0000-0002-1858-8397

Pravin H. Bhoite − *Department of Chemistry, Kisan Veer Mahavidyalaya, Wai 412803 Maharashtra, India*

Complete contact information is available at: https://pubs.acs.org/10.1021/acsaem.1c00367

Notes

The authors declare no competing financial interest.

ACKNOWLEDGMENTS

The National Research Foundation of Korea (NRF) has funded this research (NRF-2017R1A2B4008117). This work has also been sponsored by the Priority Research Centers Program, funded by the Ministry of Education, Science and Technology through the National Research Foundation of Korea (NRF) (NRF-2018R1A6A1A03024334). A.K. and P.Y extend their appreciation to the Deanship of Scientific Research at King Khalid University for funding this work through research group program under grant number RGP2/86/42.

REFERENCES

(1) Kim, J. Y.; Lee, J.-W.; Jung, H. S.; Shin, H.; Park, N.-G. High-Efficiency Perovskite Solar Cells. *Chem. Rev.* **2020**, *120*, 7867−7918.

(2) Jena, A. K.; Kulkarni, A.; Miyasaka, T. Halide Perovskite Photovoltaics: Background, Status, and Future Prospects. *Chem. Rev.* **2019**, *119*, 3036−3103.

(3) Prochowicz, D.; Tavakoli, M. M.; Kalam, A.; Chavan, R. D.; Trivedi, S.; Kumar, M.; Yadav, P. Influence of A-Site Cations on the Open-Circuit Voltage of Efficient Perovskite Solar Cells: A Case of Rubidium and Guanidinium Additives. *J. Mater. Chem. A* **2019**, *7*, 8218−8225.

(4) Liu, M.; Johnston, M. B.; Snaith, H. J. Efficient Planar Heterojunction Perovskite Solar Cells by Vapour Deposition. *Nature* **2013**, *501*, 395−398.

(5) Lee, M. M.; Teuscher, J.; Miyasaka, T.; Murakami, T. N.; Snaith, H. J. Efficient Hybrid Solar Cells Based on Meso-Superstructured Organometal Halide Perovskites. *Science* **2012**, *338*, 643−647.

(6) Tavakoli, M. M.; Tavakoli, R.; Yadav, P.; Kong, J. A Graphene/ZnO Electron Transfer Layer Together with Perovskite Passivation Enables Highly Efficient and Stable Perovskite Solar Cells. *J. Mater. Chem. A* **2019**, *7*, 679−686.

(7) Tavakoli, M. M.; Dastjerdi, H. T.; Prochowicz, D.; Yadav, P.; Tavakoli, R.; Saliba, M.; Fan, Z. Highly Efficient and Stable Inverted Perovskite Solar Cells Using Down-Shifting Quantum Dots as a Light Management Layer and Moisture-Assisted Film Growth. *J. Mater. Chem. A* **2019**, *7*, 14753−14760.

(8) Tavakoli, M. M.; Tsui, K.-H.; Zhang, Q.; He, J.; Yao, Y.; Li, D.; Fan, Z. Highly Efficient Flexible Perovskite Solar Cells with Antireflection and Self-Cleaning Nanostructures. *ACS Nano* **2015**, *9*, 10287−10295.

(9) Prochowicz, D.; Runjhun, R.; Tavakoli, M. M.; Yadav, P.; Saski, M.; Alanazi, A. Q.; Kubicki, D. J.; Kaszkur, Z.; Zakeeruddin, S. M.; Lewiński, J.; Grätzel, M. Engineering of Perovskite Materials Based on Formamidinium and Cesium Hybridization for High-Efficiency Solar Cells. *Chem. Mater.* **2019**, *31*, 1620−1627.

(10) Sanchez, S.; Hua, X.; Phung, N.; Steiner, U.; Abate, A. Flash Infrared Annealing for Antisolvent-Free Highly Efficient Perovskite Solar Cells. *Adv. Energy Mater.* **2018**, *8*, 1702915.
(11) Barrows, A. T.; Pearson, A. J.; Kwak, C. K.; Dunbar, A. D. F.; Buckley, A. R.; Lidzey, D. G. Efficient Planar Heterojunction Mixed-Halide Perovskite Solar Cells Deposited via Spray-Deposition. *Energy Environ. Sci.* **2014**, *7*, 2944−2950.
(12) Yin, J.; Qu, H.; Cao, J.; Tai, H.; Li, J.; Zheng, N. Vapor-Assisted Crystallization Control toward High Performance Perovskite Photovoltaics with over 18% Efficiency in the Ambient Atmosphere. *J. Mater. Chem. A* **2016**, *4*, 13203−13210.
(13) Tavakoli, M. M.; Yadav, P.; Prochowicz, D.; Tavakoli, R.; Saliba, M. Multilayer Evaporation of MAFAPbI 3− x Cl x for the Fabrication of Efficient and Large-Scale Device Perovskite Solar Cells. *J. Phys. D: Appl. Phys.* **2019**, *52*, 034005.
(14) Mhamad, S. A.; Mohammed, A. M.; Aziz, M.; Aziz, F. Impact of Electron Transport Layers (ETLs) and Hole Transport Layer (HTLs) on Perovskite Solar Cells Performance. *Nanostructured Materials for Next-Generation Energy Storage and Conversion: Photovoltaic and Solar Energy*; Springer Berlin Heidelberg, 2019; pp 227−246.
(15) Chen, G.-S.; Chen, Y.-C.; Lee, C.-T.; Lee, H.-Y. Performance Improvement of Perovskite Solar Cells Using Electron and Hole Transport Layers. *Sol. Energy* **2018**, *174*, 897−900.
(16) Yin, X.; Song, Z.; Li, Z.; Tang, W. Toward Ideal Hole Transport Materials: A Review on Recent Progress in Dopant-Free Hole Transport Materials for Fabricating Efficient and Stable Perovskite Solar Cells. *Energy Environ. Sci.* **2020**, *13*, 4057−4086.
(17) Yadav, P.; Dar, M. I.; Arora, N.; Alharbi, E. A.; Giordano, F.; Zakeeruddin, S. M.; Grätzel, M. The Role of Rubidium in Multiple-Cation-Based High-Efficiency Perovskite Solar Cells. *Adv. Mater.* **2017**, *29*, 1701077.
(18) Yang, B.; Suo, J.; Mosconi, E.; Ricciarelli, D.; Tress, W.; De Angelis, F.; Kim, H.-S.; Hagfeldt, A. Outstanding Passivation Effect by a Mixed-Salt Interlayer with Internal Interactions in Perovskite Solar Cells. *ACS Energy Lett.* **2020**, *5*, 3159−3167.
(19) Kim, G.; Min, H.; Lee, K. S.; Lee, D. Y.; Yoon, S. M.; Seok, S. I. Il. Impact of Strain Relaxation on Performance of A-Formamidinium Lead Iodide Perovskite Solar Cells. *Science* **2020**, *370*, 108−112.
(20) Chung, J.; Shin, S. S.; Kim, G.; Jeon, N. J.; Yang, T.-Y.; Noh, J. H.; Seo, J. Impact of Electrode Materials on Process Environmental Stability of Efficient Perovskite Solar Cells. *Joule* **2019**, *3*, 1977−1985.
(21) Giordano, F.; Abate, A.; Correa Baena, J. P.; Saliba, M.; Matsui, T.; Im, S. H.; Zakeeruddin, S. M.; Nazeeruddin, M. K.; Hagfeldt, A.; Graetzel, M. Enhanced Electronic Properties in Mesoporous TiO2 via Lithium Doping for High-Efficiency Perovskite Solar Cells. *Nat. Commun.* **2016**, *7*, 10379.
(22) Chavan, R. D.; Yadav, P.; Nimbalkar, A.; Bhoite, S. P.; Bhosale, P. N.; Kook Hong, C. Ruthenium Doped Mesoporous Titanium Dioxide for Highly Efficient, Hysteresis-Free and Stable Perovskite Solar Cells. *Sol. Energy* **2019**, *186*, 156−165.
(23) Zhen, C.; Wu, T.; Chen, R.; Wang, L.; Liu, G.; Cheng, H.-M. Strategies for Modifying TiO 2 Based Electron Transport Layers to Boost Perovskite Solar Cells. *ACS Sustainable Chem. Eng.* **2019**, *7*, 4586−4618.
(24) Lee, Y. H.; Luo, J.; Son, M.-K.; Gao, P.; Cho, K. T.; Seo, J.; Zakeeruddin, S. M.; Grätzel, M.; Nazeeruddin, M. K. Enhanced Charge Collection with Passivation Layers in Perovskite Solar Cells. *Adv. Mater.* **2016**, *28*, 3966−3972.
(25) Hwang, I.; Baek, M.; Yong, K. Core/Shell Structured TiO 2 /CdS Electrode to Enhance the Light Stability of Perovskite Solar Cells. *ACS Appl. Mater. Interfaces* **2015**, *7*, 27863−27870.
(26) Ito, S.; Tanaka, S.; Manabe, K.; Nishino, H. Effects of Surface Blocking Layer of Sb2S3 on Nanocrystalline TiO2 for CH3NH3PbI3 Perovskite Solar Cells. *J. Phys. Chem. C* **2014**, *118*, 16995−17000.
(27) Chavan, R. D.; Tavakoli, M. M.; Prochowicz, D.; Yadav, P.; Lote, S. S.; Bhoite, S. P.; Nimbalkar, A.; Hong, C. K. Atomic Layer Deposition of an Effective Interface Layer of TiN for Efficient and Hysteresis-Free Mesoscopic Perovskite Solar Cells. *ACS Appl. Mater. Interfaces* **2020**, *12*, 8098−8106.
(28) Kim, M.-K.; Kim, W.-H.; Lee, T.; Kim, H. Growth Characteristics and Electrical Properties of Ta2O5 Grown by Thermal and O3-Based Atomic Layer Deposition on TiN Substrates for Metal−Insulator−Metal Capacitor Applications. *Thin Solid Films* **2013**, *542*, 71−75.
(29) Lee, J.; Lu, W. D.; Kioupakis, E. Electronic and Optical Properties of Oxygen Vacancies in Amorphous Ta2O5 from First Principles. *Nanoscale* **2017**, *9*, 1120−1127.
(30) Fincham, C. J. B.; Lupfer, D. A. The Properties of Tantalum Oxide in Electrolytic Capacitors. *EI Electrical Insulation Conference Materials and Application, EIC 1962*; Institute of Electrical and Electronics Engineers Inc., 1962; pp 185−189.
(31) Narangari, P. R.; Karuturi, S. K.; Wu, Y.; Wong-Leung, J.; Vora, K.; Lysevych, M.; Wan, Y.; Tan, H. H.; Jagadish, C.; Mokkapati, S. Ultrathin Ta 2 O 5 Electron-Selective Contacts for High Efficiency InP Solar Cells. *Nanoscale* **2019**, *11*, 7497−7505.
(32) Bartic, C.; Jansen, H.; Campitelli, A.; Borghs, S. Ta2O5 as Gate Dielectric Material for Low-Voltage Organic Thin-Film Transistors. *Org. Electron.* **2002**, *3*, 65−72.
(33) Seo, S.; Jeong, S.; Park, H.; Shin, H.; Park, N.-G. Atomic Layer Deposition for Efficient and Stable Perovskite Solar Cells. *Chem. Commun.* **2019**, *55*, 2403−2416.
(34) Deng, K.; Li, L. Advances in the Application of Atomic Layer Deposition for Organometal Halide Perovskite Solar Cells. *Adv. Mater. Interfaces* **2016**, *3*, 1600505.
(35) Kim, M.-K.; Kim, W.-H.; Lee, T.; Kim, H. Growth Characteristics and Electrical Properties of Ta2O 5 Grown by Thermal and O3-Based Atomic Layer Deposition on TiN Substrates for Metal-Insulator-Metal Capacitor Applications. *Thin Solid Films* **2013**, *542*, 71−75.
(36) Henke, T.; Knaut, M.; Geidel, M.; Winkler, F.; Albert, M.; Bartha, J. W. Atomic Layer Deposition of Tantalum Oxide Thin Films Using the Precursor Tert-Butylimido-Tris-Ethylmethylamido-Tantalum and Water: Process Characteristics and Film Properties. *Thin Solid Films* **2017**, *627*, 94−105.
(37) Chavan, R. D.; Prochowicz, D.; Yadav, P.; Tavakoli, M. M.; Nimbalkar, A.; Bhoite, S. P.; Hong, C. K. Effect of CsCl Additive on the Morphological and Optoelectronic Properties of Formamidinium Lead Iodide Perovskite. *Sol. RRL* **2019**, *3*, 1900294.
(38) Cho, K. T.; Paek, S.; Grancini, G.; Roldán-Carmona, C.; Gao, P.; Lee, Y.; Nazeeruddin, M. K. Highly Efficient Perovskite Solar Cells with a Compositionally Engineered Perovskite/Hole Transporting Material Interface. *Energy Environ. Sci.* **2017**, *10*, 621−627.
(39) Tavakoli, M. M.; Giordano, F.; Zakeeruddin, S. M.; Grätzel, M. Mesoscopic Oxide Double Layer as Electron Specific Contact for Highly Efficient and UV Stable Perovskite Photovoltaics. *Nano Lett.* **2018**, *18*, 2428−2434.
(40) Chavan, R. D.; Parikh, N.; Tavakoli, M. M.; Prochowicz, D.; Kalam, A.; Yadav, P.; Bhoite, P. H.; Hong, C. K. Mesoscopic TiO_2 /Nb_2O_5 Electron Transfer Layer for Efficient and Stable Perovskite Solar Cells. *Adv. Mater. Interfaces* **2021**, *8*, 2100177.
(41) Kang, J.; Yun, S.; Park, S.; Kim, Y. Effect of Rapid Thermal Annealing on the Structure and the Electrical Properties of Atomic-Layer-Deposited Ta2O5 Films. *J. Kor. Phys. Soc.* **2000**, *37*, 975−979.
(42) Lee, C.-C.; Tang, C.-J. TiO2 - Ta2O5 Composite Thin Films Deposited by Radio Frequency Ion-Beam Sputtering. *Appl. Opt.* **2006**, *45*, 9125−9131.
(43) Prusakova, V.; Collini, C.; Lunelli, L.; Vanzetti, L.; Chiappini, A.; Lorenzelli, L.; Pederzolli, C.; Chiasera, A.; Ferrari, M.; Dirè, S. Towards Low Voltage Resistive Switch in Sol-Gel Derived TiO2/Ta2O5 Stack Thin Films. *Mater. Des.* **2016**, *105*, 359−365.
(44) Lee, C.-C.; Tang, C.-J. TiO2 - Ta2O5 Composite Thin Films Deposited by Radio Frequency Ion-Beam Sputtering. *Appl. Opt.* **2006**, *45*, 9125−9131.
(45) Kim, H.-S.; Park, N.-G. Parameters Affecting I − V Hysteresis of $CH_3NH_3PbI_3$ Perovskite Solar Cells: Effects of Perovskite Crystal Size and Mesoporous TiO_2 Layer. *J. Phys. Chem. Lett.* **2014**, *5*, 2927−2934.

https://doi.org/10.1021/acsaem.1c00367
ACS Appl. Energy Mater. 2021, 4, 10433−10441

(46) Yadav, P.; Turren-Cruz, S.-H.; Prochowicz, D.; Tavakoli, M. M.; Pandey, K.; Zakeeruddin, S. M.; Grätzel, M.; Hagfeldt, A.; Saliba, M. Elucidation of Charge Recombination and Accumulation Mechanism in Mixed Perovskite Solar Cells. *J. Phys. Chem. C* **2018**, *122*, 15149−15154.
(47) Liu, P.; Wang, W.; Liu, S.; Yang, H.; Shao, Z. Fundamental Understanding of Photocurrent Hysteresis in Perovskite Solar Cells. *Adv. Energy Mater.* **2019**, *9*, 1803017.
(48) Kang, D. H.; Park, N. G. On the Current−Voltage Hysteresis in Perovskite Solar Cells: Dependence on Perovskite Composition and Methods to Remove Hysteresis. *Adv. Mater.* **2019**, *31*, 1805214.
(49) Pool, V. L.; Dou, B.; Van Campen, D. G.; Klein-Stockert, T. R.; Barnes, F. S.; Shaheen, S. E.; Ahmad, M. I.; van Hest, M. F. A. M.; Toney, M. F. Thermal Engineering of FAPbI3 Perovskite Material via Radiative Thermal Annealing and in Situ XRD. *Nat. Commun.* **2017**, *8*, 14075.
(50) Jeong, J.; Kim, M.; Seo, J.; Lu, H.; Ahlawat, P.; Mishra, A.; Yang, Y.; Hope, M. A.; Eickemeyer, F. T.; Kim, M.; Yoon, Y. J.; Choi, I. W.; Darwich, B. P.; Choi, S. J.; Jo, Y.; Lee, J. H.; Walker, B.; Zakeeruddin, S. M.; Emsley, L.; Rothlisberger, U.; Hagfeldt, A.; Kim, D. S.; Grätzel, M.; Kim, J. Y. Pseudo-Halide Anion Engineering for α-$FAPbI_3$ Perovskite Solar Cells. *Nature* **2021**, *592*, 381−385.
(51) Nie, W.; Tsai, H.; Asadpour, R.; Blancon, J.-C.; Neukirch, A. J.; Gupta, G.; Crochet, J. J.; Chhowalla, M.; Tretiak, S.; Alam, M. A.; Wang, H.-L.; Mohite, A. D. High-Efficiency Solution-Processed Perovskite Solar Cells with Millimeter-Scale Grains. **2015**, *347* (), 522−525. DOI: 10.1126/science.aaa0472
(52) Sherkar, T. S.; Momblona, C.; Gil-Escrig, L.; Ávila, J.; Sessolo, M.; Bolink, H. J.; Koster, L. J. A. Recombination in Perovskite Solar Cells: Significance of Grain Boundaries, Interface Traps, and Defect Ions. *ACS Energy Lett.* **2017**, *2*, 1214−1222.
(53) Carrillo, J.; Guerrero, A.; Rahimnejad, S.; Almora, O.; Zarazua, I.; Mas-Marza, E.; Bisquert, J.; Garcia-Belmonte, G. Ionic Reactivity at Contacts and Aging of Methylammonium Lead Triiodide Perovskite Solar Cells. *Adv. Energy Mater.* **2016**, *6*, 1502246.
(54) Ke, W.; Stoumpos, C. C.; Logsdon, J. L.; Wasielewski, M. R.; Yan, Y.; Fang, G.; Kanatzidis, M. G. TiO_2 −ZnS Cascade Electron Transport Layer for Efficient Formamidinium Tin Iodide Perovskite Solar Cells. *J. Am. Chem. Soc.* **2016**, *138*, 14998−15003.
(55) Ma, J.; Guo, X.; Zhou, L.; Lin, Z.; Zhang, C.; Yang, Z.; Lu, G.; Chang, J.; Hao, Y. Enhanced Planar Perovskite Solar Cell Performance via Contact Passivation of TiO 2 /Perovskite Interface with NaCl Doping Approach. **2018**, *1*. 3826 https://doi.org/ DOI: 10.1021/acsaem.8b00602.
(56) Shaikh, S. F.; Kwon, H.-C.; Yang, W.; Hwang, H.; Lee, H.; Lee, E.; Ma, S.; Moon, J. La2O3 Interface Modification of Mesoporous TiO2 Nanostructures Enabling Highly Efficient Perovskite Solar Cells. *J. Mater. Chem. A* **2016**, *4*, 15478.
(57) Chavan, R. D.; Yadav, P.; Tavakoli, M. M.; Prochowicz, D.; Nimbalkar, A.; Bhoite, S. P.; Bhosale, P. N.; Hong, C. K. Double Layer Mesoscopic Electron Contact for Efficient Perovskite Solar Cells. *Sustainable Energy Fuels* **2020**, *4*, 843−851.
(58) Srinivasa Rao, S.; Punnoose, D.; Venkata Tulasivarma, C.; Pavan Kumar, C. H. S. S.; Gopi, C. V. V. M.; Kim, S.-K.; Kim, H.-J. A Strategy to Enhance the Efficiency of Dye-Sensitized Solar Cells by the Highly Efficient TiO_2 /ZnS Photoanode. *Dalton Trans.* **2015**, *44*, 2447−2455.
(59) Ke, W.; Stoumpos, C. C.; Logsdon, J. L.; Wasielewski, M. R.; Yan, Y.; Fang, G.; Kanatzidis, M. G. TiO2-ZnS Cascade Electron Transport Layer for Efficient Formamidinium Tin Iodide Perovskite Solar Cells. *J. Am. Chem. Soc.* **2016**, *138*, 14998−15003.
(60) Feng, X.; Shankar, K.; Paulose, M.; Grimes, C. A. Tantalum-Doped Titanium Dioxide Nanowire Arrays for Dye-Sensitized Solar Cells with High Open-Circuit Voltage. *Angew. Chem., Int. Ed.* **2009**, *48*, 8095−8098.
(61) Shi, X.; Chen, R.; Jiang, T.; Ma, S.; Liu, X.; Ding, Y.; Cai, M.; Wu, J.; Dai, S. Regulation of Interfacial Charge Transfer and Recombination for Efficient Planar Perovskite Solar Cells. *Sol. RRL* **2020**, *4*, 1900198.
(62) Sung, Y.-M.; Akbar, A. K.; Biring, S.; Li, C.-F.; Huang, Y.-C.; Liu, S.-W. The Effect of ZnO Preparation on the Performance of Inverted Polymer Solar Cells under One Sun and Indoor Light. *J. Mater. Chem. C* **2021**, *9*, 1164.
(63) Tress, W.; Yavari, M.; Domanski, K.; Yadav, P.; Niesen, B.; Correa Baena, J. P.; Hagfeldt, A.; Graetzel, M. Interpretation and Evolution of Open-Circuit Voltage, Recombination, Ideality Factor and Subgap Defect States during Reversible Light-Soaking and Irreversible Degradation of Perovskite Solar Cells. *Energy Environ. Sci.* **2018**, *11*, 151−165.
(64) Dunfield, S. P.; Bliss, L.; Zhang, F.; Luther, J. M.; Zhu, K.; Hest, M. F. A. M.; Reese, M. O.; Berry, J. J. From Defects to Degradation: A Mechanistic Understanding of Degradation in Perovskite Solar Cell Devices and Modules. *Adv. Energy Mater.* **2020**, *10*, 1904054.
(65) Zhao, Z.; Gu, F.; Rao, H.; Ye, S.; Liu, Z.; Bian, Z.; Huang, C. Metal Halide Perovskite Materials for Solar Cells with Long-Term Stability. *Adv. Energy Mater.* **2019**, *9*, 1802671.
(66) Tavakoli, M. M.; Yadav, P.; Tavakoli, R.; Kong, J. Surface Engineering of TiO_2 ETL for Highly Efficient and Hysteresis-Less Planar Perovskite Solar Cell (21.4%) with Enhanced Open-Circuit Voltage and Stability. *Adv. Energy Mater.* **2018**, *8*, 1800794.
(67) Sachs, M.; Pastor, E.; Kafizas, A.; Durrant, J. R. Evaluation of Surface State Mediated Charge Recombination in Anatase and Rutile TiO 2. **2016**, *7*. 3742 https://doi.org/ DOI: 10.1021/acs.jpclett.6b01501.
(68) Zhang, M.; Zhou, W.; Hu, W.; Li, B.; Qiao, Q.; Yang, S. Modifying Mesoporous TiO2 by Ammonium Sulfonate Boosts Performance of Perovskite Solar Cells. *ACS Appl. Mater. Interfaces* **2020**, *12*, 12696−12705.